Lawrence Berkeley National Laboratory

Title

A Microscopic Calculation of Fragment Formation in Nucleus-Nucleus Collisions

Permalink

https://escholarship.org/uc/item/1d8571mf

Author

Harvey, B G

Publication Date

1985

Copyright Information

Lawrence Berkeley Laboratory
UNIVERSITY OF CALIFORNIA

A MICROSCOPIC CALCULATION OF FRAGMENT FORMATION
IN NUCLEUS-NUCLEUS COLLISIONS

B.G. Harvey

January 1985

DISCLAIMER

A MICROSCOPIC CALCULATION OF FRAGMENT FORMATION
IN NUCLEUS-NUCLEUS COLLISIONS*

Bernard G. Harvey

Nuclear Science Division
Lawrence Berkeley Laboratory
University of California
Berkeley, CA   94720

January 1985

A MICROSCOPIC CALCULATION OF FRAGMENT FORMATION
IN NUCLEUS-NUCLEUS COLLISIONS*

Bernard G. Harvey

Nuclear Science Division
Lawrence Berkeley Laboratory
University of California
Berkeley, CA 94720

ABSTRACT

A microscopic model using effective and free nucleon-nucleon scattering cross sections is used to calculate the yields of projectile-like fragments from nucleus-nucleus collisons from 20 MeV/A to 2 GeV/A. Good agreement with reaction cross section and fragment cross section measurements is obtained. The enhanced yields of neutron-rich fragments observed experimentally at low beam energies from collisions of projectiles with heavy targets are reproduced somewhat better by the inclusion of a neutron-rich surface on the heavy target nuclei. Each fragment mass is produced in a strongly localized region of the distance of closest approach between the colliding nuclei; lighter fragments come from small distances and heavier ones from more peripheral collisions.

I. Introduction

Soon after beams of heavy ions of 20 MeV/A and 2 GeV/A became available from the 88-Inch Cyclotron and the Bevalac at Berkeley, an unexpectedly strong similarity was found between nucleus-nucleus collisions at these two widely different energies[1]. In particular, the yields of projectile-like fragments (PLF), when summed by atomic number Z, were nearly the same for 20 MeV/A and for 2 GeV/A ions of ^{16}O colliding with a target of ^{208}Pb.

With a heavy target nucleus such as ^{208}Pb, there were nevertheless consistent differences in the yields of individual isotopes. The neutron-excess isotopes were produced in greater yields at 20 MeV/A than at 2 GeV/A.

At 20 MeV/A, the yields of neutron-excess fragments were greater from a target of ^{208}Pb than from the less neutron-rich target ^{94}Zr[1]. At 2 GeV/A, though, there was no such effect in the comparison of yields from targets of Cu and Pb[1]. The comparison of yields from ^{20}Ne + ^{197}Au (290 MeV) with those from ^{20}Ne + ^{58}Ni (270 MeV) shows again a large enhancement of the neutron-excess isotopes from the ^{197}Au target [2]. This result has been discussed by Homeyer[3].

Thus it seems reasonably well established that the large extra yields of neutron-rich isotopes at lower projectile energies are associated with large values of the neutron to proton ratio N/Z of the target. At 2 GeV/A, these extra yields are not observed, even from extremely neutron-rich targets.

It is tempting to associate these observations with the energy dependence of the nucleon-nucleon cross sections shown in Fig. 1. At low energies, σ_{np} is three times larger than σ_{nn} and σ_{pp}. Therefore, projectile protons are more likely to be scattered from target nucleons than are projectile neutrons when the target has N > Z. If this scattering removes nucleons from the projectile to form the PLF, the PLF's should be proton-deficient and therefore neutron-rich. At ~ 500 MeV (lab) and beyond, σ_{np} becomes approximately equal to σ_{nn} (σ_{pp}) so that the N/Z ratio of the target is no longer of importance. With the assumption that the removal of nucleons from the projectile to form the PLF occurs only through these nucleon-nucleon (N-N) scatterings, it is clear that the trends of the N-N cross sections are in the right direction to account qualitatively for the experimental results.

It is by now well established that the drop in the reaction cross section σ_r between many colliding nuclei observed at energies beyond ~ 20 MeV/A can be quantitatively explained by the energy dependence of the N-N cross sections [4-8]. The microscopic calculations of refs. 5-7 are extremely elaborate. They take into account the effects of the Fermi motion of the nucleons in the collision partners, as well as the Pauli blocking of elementary scatterings in which one or both of the nucleons remain below the Fermi surface. Nevertheless, calculations without Fermi motion and Pauli blocking gave values of σ_r in agreement with experiment even at energies as low as 20 MeV/A [6,8,9]. Therefore it seemed worthwhile to make the simplest possible calculation to see to what extent the N-N cross sections might account for the experimental

observations of PLF yields described above. Cole[10], using a method similar to that of Karol[11], has developed an analytic calculation of PLF yields. The present calculation uses Monte Carlo methods which, although slower, permit the inclusion of more realistic nuclear density distributions for protons and neutrons.

II. The Calculations

The two colliding nuclei are asumed to have spherically symmetric Fermi density distributions. The radius and diffusivity of the neutron distribution is usually different from that of the proton distribution in order to allow the use of a neutron-rich surface in the heavy target nuclei. The projectile follows a path in the Coulomb plus nuclear potential with impact parameter b until the 10% densities of the two nuclei overlap. When, at large values of b, the nuclear density overlap cannot reach the 10% value, the distance of closest approach D is that of a pure Coulomb orbit. Thereafter, the projectile nucleons follow straight paths into and through the target.

Thus the effect of the combined nuclear and Coulomb potentials of the two colliding nuclei on the paths of the individual projectile nucleons is ignored. To a certain degree, the action of the two attractive potential wells tends to cancel, for if a projectile nucleon were deflected by the target potential towards the target center, it would be pulled away from the attractive projectile potential and vice versa.

It is assumed that any projectile nucleon that scatters from a target

nucleon will be permanently removed from the projectile, and that no nucleons are scattered back into bound states of the PLF. The number of scattered nucleons is calculated by Monte Carlo techniques.

The geometry of the collision is shown in fig. 2. In the spherical coordinate system, the element of volume is $d(r^3/3)d(\cos\theta)d\psi$. The radius r_1 of a nucleon in the projectile of mass A_1 is therefore obtained by choosing r_1^3 at random in the interval 0 to 17 A_1, well out into the low density tail of the distribution. The projectile proton or neutron density at r_1 is then calculated and the value of r_1 is either accepted or rejected in such a way as to reflect the projectile proton or neutron density at r_1. Next, the cosine of the angle θ is chosen randomly in the interval -1 to +1, and the angle ϕ in the interval 0 to 2π. In order to preserve the centers of mass and charge of the projectile, the coordinates of alternate neutrons and protons are obtained by reflecting those of the previous neutron or proton about the center of the projectile. The distance R betwen the point P and the target center is then obtained from:-

$$R = [(D-r)^2 + (Z-c\cos\phi)^2 + c^2\sin^2\phi]^{1/2} \qquad (1)$$

where r equals $r_1\cos\theta$.

The target neutron and proton densities at P are then calculated. The length Z is next stepped along the straight path and the target neutron and proton densities are recalculated at each new value of R.

If the projectile nucleon is a proton, the probability that it will not scatter from a target neutron or proton as it moves along the Z-direction is:

$$P_p = \exp - (\int \rho_n(R)\sigma_{pn}(R)dZ + \int \rho_p(R)\sigma_{pp}(R)dZ) \qquad (2)$$

For a projectile neutron, the corresponding probability is:-

$$P_n = \exp - (\int \rho_n(R)\sigma_{nn}(R)dZ + \int \rho_p(R)\sigma_{np}(R)dZ) \qquad (3)$$

Here, $\rho_n(R)$ and $\rho_p(R)$ are the target neutron and proton densities at each point along the trajectory. The subscripts (p or n) on the cross sections σ refer in order to the projectile nucleon and the target nucleon. As discussed below, the effective nucleon-nucleon cross sections are allowed to vary with the target density and hence with the value of R, the distance of the projectile nucleon from the center of the target nucleus. The integrals are evaluated by Simpson's rule in 7 intervals of $(Z - c \cos\phi)$ from 0 to +14 fm and then doubled to obtain their values from -14 to +14 fm.

For each probability P_p or P_n, a decision is then made as to whether or not the nucleon scattered, by generating a random number N in the interval 0-1/P. In $N \geqslant 1$, a scattering is assumed to have happened. This procedure is repeated Z_1 times (protons) and N_1 times (neutrons) to obtain the number of protons and neutrons scattered out of the projectile, and hence the charge Z_3 and neutron number N_3 of the PLF. This is then repeated 2000-3000 times for each of 21 value of b from 0 to a value beyond which there are no more nucleon-nucleon scatterings.

Since Fermi motion and Pauli blocking are not explicitly included in the calculation, the values of σ_{nn} and σ_{np} at the lower energies have

to be treated as parameters whose values ought to be smaller than the free nucleon-nucleon scattering cross sections, but with the ratio σ_{nn}/σ_{np} equal to that of the free N-N values.

It is well known that Pauli blocking is reduced in the low density nuclear surface [7]. Using the Reid hard core potential, Jeukenne et al.[12] found that the value of W_0/ρ varied approximately as $1/\rho$ for projectiles of 10-50 MeV. Here, W_0 is the imaginary isoscalar component of the optical potential. Since $W_0/\rho \propto \sigma_{NN}$, this result suggests that σ_{NN} should be roughly proportional to $1/\rho$. At 140 MeV, W_0/ρ was found to be almost independent of ρ so that σ_{NN} should be constant throughout the nuclear volume.

The detailed calculations of DiGiacomo et al.[7] show that the effective N-N cross sections reach the free values for projectile nucleons of only 20 MeV in the target surface region where the Fermi momentum k_f equals 0.5 fm^{-1}. This value corresponds to a density of about 5% of the central value. For projectile energies > 150 MeV, the effective cross sections were found to be very nearly equal to the free values at all values of k_f and hence of the density. As expected, Pauli blocking of the collisions has no effect at energies well above the Fermi energy.

These results suggest a very simple approximation for the radial dependence of the effective cross sections at energies below or not far above the Fermi energy. In the central region, σ_{nn} and σ_{np} were given values that correspond to experimental[13] and calculated [14,15] values of the nucleon mean free path, with the ratio

σ_{np}/σ_{NN} equal to 3, the ratio for the free nucleon-nucleon cross sections. These central region values were allowed to increase as $1/\rho_{tgt}$ up to the free values in the low density tail of the target nucleus. Thus the effective cross sections are functions of R in eqs. 2 and 3. At 2 GeV/A on the other hand, Pauli blocking should have a negligible effect even in the target center region. The free N-N values were therefore used throughout the nuclear volume. The choice of the central effective cross sections has only a minor effect on the PLF cross sections and none at all on the reaction cross section.

Experimental values of PLF cross sections are observed to be larger for the more stable fragments. For example, the cross section for formation of ^{16}O from a ^{20}Ne projectile is substantially larger than for the formation of ^{15}O. This very general observation led Friedman [16] to suggest that cross sections depend on the probability that the PLF and the nucleons removed from the projectile to form that PLF will be found at a certain minimum distance from each other. This probability P_f depends approximately on the separation energy of the projectile into the PLF and the removed nucleons.

Its value is given by:-

$$P_f = \frac{\exp - (B\mu x_0)}{(1-B) \, x_0^3} \tag{4}$$

where B is a parameter whose value, following ref. 17, was set equal to 0.3 and:-

$$\mu = [E_s A_3 (A_1 - A_3)/A_1]^{1/2}$$
$$x_0 = 1.2 \, A_3^{1/3} \quad : \quad A_3 \geqslant A_1/2 \tag{5}$$
$$x_0 = 1.2 \, (A_1 - A_3)^{1/3} : A_3 < A_1/2$$

A_1, A_3 are the projectile and PLF masses respectively, and E_s is

the minimum energy required to separate A_1 into the PLF A_3 and the residue (A_1-A_3).

In addition, Friedman includes a "spectroscopic factor" that expresses the probability that the number of nucleons removed from the projectile will be divided in a given way between neutrons and protons. The Monte Carlo procedure automatically reproduces this "spectroscopic factor", and it is therefore not necessary to include it explicitly.

For each value of the impact parameter b, the cross sections $\sigma_b(Z,N)$ for the formation of the various PLF's are renormalized by their Friedman probabilities P_f as follows:-

$$\sigma_b(Z,N) = \frac{2\pi b db\ N(Z,N)\ P_f(Z,N)}{\sum\limits_{Z,N} N(Z,N)\ P_f(Z,N)} \tag{6}$$

Here, $N(Z,N)$ is the number of events producing the PLF (Z,N) at impact parameter b, and $P_f(Z,N)$ is the Friedman probability for formation of that PLF. The sum runs over the (Z,N) values for all the PLF's formed at b. The total cross section for formation of PLF(Z,N) is just the sum of the $\sigma_b(Z,N)$ over all values of b. The reaction cross section is calculated from:-

$$\sigma_r = \sum\limits_b 2\pi b db\ N(react)/N \tag{7}$$

$N(react)/N$ is the fraction of events at each value of b that lead to a PLF different in mass from the projectile, i.e. to a reaction.

The value of P_f is not defined for those events in which every nucleon
of the projectile suffers a scattering and no PLF emerges. At low beam
energies, these events would correspond to complete fusion of projectile and
target. P_f for "complete fusion" is set equal to 1, a value which is very
much larger than for any other PLF. This procedure has been found to
reproduce very well the complete fusion cross sections at low projectile
energies [17]. As will be seen later, this "complete fusion" process
occurs only at small values of the impact parameter where the competing PLF
channels are such light fragments as neutrons and the isotopes of hydrogen
and helium for which there are few experimental cross sections. The
arbitrary choice of this value of P_f for "complete fusion" has no effect on
σ_r or on the cross sections for the heavier PLF's, since these are formed
at larger impact parameters where there are no longer any "complete fusion"
events.

III. Results of the Calculations

1. Reaction Cross Sections

The reaction cross section of the system $^{12}C + {}^{12}C$ has been measured
experimentally over a very wide energy range [18] and calculated by
DiGiacomo et al.[8]. The present calculation immediately showed that, as
might well be expected, the value of σ_r depends only on the values of the
free nucleon-nucleon scattering cross sections in the surface region.
Changing the Pauli-blocked central region cross sections changes the cross
sections for the formation of the light PLF's by a small amount but it has no
effect on the reaction cross section as long as the center region is not so
transparent that all the projectile nucleons pass through it.

Figure 3 shows a comparison of the calculated values of σ_r with experiment and with the calculations of DiGiacomo et al [8]. The agreement is excellent. The parameters of the calculation are shown in Table 1. For the system ^{16}O + ^{208}Pb, the calculated values of σ_r are 3333 mb at 20 MeV/A and 3606 mb at 2 GeV/A. The experimental value is 3400 mb at 20 MeV/A [1]. Thus the Monte Carlo calculation agrees with experiment to 2%. The value at 2 GeV/A is expected to be higher. At lower energies, the large Coulomb repulsion pushes the peripheral partial waves of the projectile away from the surface of the target nucleus, thus reducing the range of impact parameters within which reactions can take place. In the parameterization of Kox et al. [20], this effect is expressed by making σ_r proportional to (1-V/E), where V is the height of the Coulomb barrier and E is the c.m. energy.

For the system ^{20}Ne + ^{197}Au (20 MeV/A), the calculated value of σ_r is 3460 mb, within 2.3% of the experimental value of 3540±50 mb [20]. For ^{40}Ar + ^{197}Au at 44 MeV/A, the calculated value of σ_r is 4290 mb. The experimental value is 4410 ± 120 mb [21]. Thus the calculated and experimental values agree within the error limits.

2. Fragment Cross Sections.

a. The excitation energy of primary fragments.

The Monte Carlo calculations give the cross sections for forming the

primary fragments but with no information about their excitation energies. Comparison with experimental inclusive cross sections, though, requires the calculated cross sections to be corrected for the decay of any excited primary PLF's. It is therefore necessary to discuss at some length the meager experimental measurements of PLF excitations and the models that are commonly used to predict them, before comparing the experimental and calculated cross sections in the following sections.

It will be shown that the experimental evidence at beam energies up to ~20 MeV/A suggest that the PLF excitation energies are surprisingly low, and that there is weaker evidence that the excitations remain low up to beams of 2 GeV/A. Moreover, the models that predict large excitation energies will be shown to be either unreliable or to have been incorrectly used.

There are few measurements of the spectrum of excitation energy carried by the primary PLF's. For the system ^{20}Ne + ^{197}Au at 220 and 340 MeV [22] and, ^{16}O + CsI at 260 MeV [23], the multiplicity of charged particles in coincidence with PLF's is very low. In fact, a substantial fraction of the PLF's are not in coincidence with any charged particles at all, which shows that the PLF excitation energy frequently lies below the first particle decay threshold, which is in most cases for proton or alpha particle emission at some 5-10 MeV. The next most common events are coincidences between a PLF and just one additional charged particle. These events are interpreted as arising from the sequential decay of PLF's that are excited to energies not far above the first decay threshold. In some high resolution studies, the decaying states have been identified [24].

At higher energies (>20 MeV/A) and for projectiles heavier than ^{20}Ne, there appear to be no measurements of the excitation energy of the primary fragments. Nevertheless, the abrasion model [23] makes predictions that have been used by some authors to correct the calculated yields of primary fragments for their subsequent decay. Two versions of the model exist [25]. In the first, the dispersion of the number of neutrons and protons that are abraded - for a fixed total mass - is given by a hypergeometric function that is similar to the "spectroscopic factor" of Friedman [16]. The mass dispersion for primary PLF's of a given Z is extremely broad, much broader than the experimental results [25,26]. The narrow experimental A-dispersion is recovered by the assumption that the primary PLF's are formed with extremely large excitation energies that lead to long evaporation chains and thus to the concentration of inclusive PLF yields into the valley of stability. There is no direct experimental evidence for these large primary PLF excitation energies.

The second version of the abrasion model assumes that the colliding nuclei make "clean cuts" in each other. For static proton and neutron density distributions, this assumption would lead to a unique ratio of the numbers of protons and neutrons abraded for a given A. Since this A-dispersion is much narrower than the experimental results, it is broadened by assuming that, as a consequence of the Gamow-Teller giant dipole mode, [27] the proton and neutron densities oscillate in time so that the numbers of each that are abraded will vary. This version of the abrasion model requires smaller - but still substantial - PLF excitations in order to obtain agreement with experimental cross sections [26].

However, the assumption that the two nuclei make "clean cuts" in one another requires that the nucleon-nucleon scattering cross sections be very large and the nuclear surfaces sharp. Especially at high energies where the abrasion model is supposed to be applicable, these cross sections are small. The Monte Carlo calculations, using realistic Fermi density distributions and experimental values for the N-N scattering cross sections, produce A-dispersions for PLF's of a given Z that are quite broad, and similar to the hypergeometric abrasion model. In the present work, it is the Friedman probabilities that make the A-distributions narrow and concentrate them into the valley of stability where the separation energies are smallest. Large PLF excitation energies are not required.

Viyogi et al.[26] measured PLF cross sections from $^{40}Ar + ^{12}C$ at 213 MeV/A and compared the results with the two versions of the abrasion model. The first (hypergeometric dispersion) required enormous primary PLF excitations in order to obtain agreement with the experimental results. This excitation energy was assumed to come from two sources, the surface energy of the deformed primary PLF [25], and the excitation of the PLF by its interaction with nucleons that scattered in the target-projectile overlap region [28,29]. This second contribution was taken by Viyogi et al. from the high energy limit of refs. 28 and 29. At 213 MeV though, nucleon-nucleon scattering is not strongly forward peaked as it is at high energies. The estimate of this source of excitation that was used by Viyogi et al. is therefore too large by a substantial factor. Moreover, Hüfner, Schäfer and Schürmann[29] concluded that the secondary excitation by scattered nucleons was not understood. They also showed that the abrasion model surface

excitaion energy for ^{12}C PLF's from ^{16}O + ^{9}Be $\rightarrow$ ^{12}C (2 GeV/A) was too large by a factor of three.

The surface excitation energies predicted by the abrasion model are much larger for PLF's from ^{40}Ar + ^{12}C than from ^{40}Ar + ^{58}Ni as fig. 4 shows. Nevertheless, the PLF cross sections from these two colliding systems are remarkably similar as Table II shows. Although it is possible that different primary PLF yields and excitations lead by chance to the same inclusive cross sections, it seems much more likely that the abrasion model surface excitations are quite unreliable and probably much too high for ^{40}Ar + ^{12}C. Guerreau et al. [30] also concluded that the excitation energy of PLF's from 44 MeV/A ^{40}Ar + ^{58}Ni or ^{197}Au is quite low.

Inclusive cross sections for ^{16}O + ^{208}Pb at 20 MeV/A [1] and 2 GeV/A [31] have been measured. For all Z-values from 3 to 7, the ratio of elemental cross sections σ_Z(20 MeV/A)/σ_Z(2GeV/A) is equal to 1.7±0.4. At the lower energy, the multiplicity of charged particles in coincidence with the PLF in the system ^{16}O + CsI is very low, nearly always either 0 or 1 [23]. This observation shows that the PLF's are produced with small excitation energies. The remarkable similarity between the inclusive element yields at 20 MeV/A and 2 GeV/A argues strongly for a similar production mechanism and low PLF excitation energies at both energies. Again, one cannot exclude the possibility that the primary PLF yields and excitation energies are quite different, but lead by chance to very similar inclusive cross sections.

A final piece of evidence, albeit over only a small energy range, comes from a measurement [32] of the ratio of the primary alpha-particles to

those that arise from sequential decay of excited PLF's in the system ^{20}Ne + ^{197}Au. Between 11 MeV/A and 20 MeV/A, this ratio is constant, suggesting that there is no change in the ratio of PLF's formed in particle-stable states to those formed in α-decaying states.

To summarize, the few direct measurements that have been made with beams in the region of 20 MeV/A suggest that the PLF excitation energies are surprisingly small. The remarkable similarity between PLF inclusive cross sections at low and high energies and from light and heavy targets strongly suggests that the PLF excitation energies do not change much between projectile energies of 20 MeV/A and 2 GeV/A (^{16}O) or between 44 MeV/A and 213 MeV/A (^{40}Ar).

b. The system ^{16}O + ^{208}Pb at 20 MeV/A and 2 GeV/A.

The discussion in the previous section shows that the PLF excitation energies at a beam energy of about 20 MeV/A are small, and that they may well also be small at 2 GeV/A. A detailed analysis of the charged particle multiplicities observed experimentally in the system ^{16}O + CsI at 17 MeV/A [23] shows that the difference between the elemental primary PLF yields and the elemental inclusive cross sections is less than 30%. Of course, the effect of sequential decay can have a greater effect on the inclusive yield of a particular isotope, but no experimental data exist that permit such a detailed analysis to be made with confidence. In fig. 5, therefore, the calculated PLF primary yields from ^{16}O + ^{208}Pb are compared with the experimental inclusive cross sections at 20 MeV/A [1] and 2 GeV/A [31]. The parameters describing the Fermi density distributions of protons and neutrons in the ^{16}O and ^{208}Pb nuclei, as well as the values

of the nucleon-nucleon scattering cross sections are shown in Table I. The calculated point for ^{4}He production at 2 GeV/A is the sum of the cross section for formation of ^{4}He as a PLF and the contributions from the decay of the unbound nuclei ^{5}He, ^{5}Li, ^{8}Be and ^{9}B. A large fraction of the ^{4}He in fact comes from the production and decay of ^{8}Be. Figure 5 shows that the agreement between experiment and calculation is generally good. The large cross sections for ^{12}C fragments at both energies come from the small separation energy of ^{16}O into ^{12}C + ^{4}He and the large value of the Friedman probability.

c. The system ^{20}Ne + ^{197}Au at 20 MeV/A.

An estimate of the primary yields of PLF's in this system at 290 MeV has been made by Homeyer et al. [33]. For several of the fragments, though, the estimated contributions to the inclusive yield that come from the sequential decay of heavier fragments exceed the measured inclusive cross section by as much as a factor of two. Moreover, the contribution of ^{20}Ne* $\rightarrow$ ^{16}O + ^{4}He to the inclusive ^{16}O yield is inconsistent with the ^{16}O alpha-multiplicity measured by the same group [34]. The average ratio of deduced primary to inclusive yield [33] is only 1.12, although there are excursions in each direction as large as a factor of 2.5 for certain PLF's.

Figure 6 therefore shows a comparison of the calculated primary PLF cross sections with the unadjusted experimental inclusive values [2]. The parameters used in the calculation are shown in Table I. Again, agreement between calculation and experiment is satisfactory.

d. The system ^{18}O + ^{48}Ti at 1.7 GeV/A.

Fragment cross sections from 1.7 GeV/A ^{18}O on several targets have been measured by Olson et al. [35]. Figure 7 shows a comparison of experimental and calculated PLF cross sections from a target of ^{48}Ti. The maximum cross section for Z = 6 occurs at masses 13-14 (experiment) and 14 (calculated). For ^{16}O projectiles (Fig. 5) the peak is at mass 12. The calculation reproduces the upward shift in mass for the Z=6 isotopes from ^{18}O. If the observed PLF's were formed through a long decay chain from highly excited primaries, such a difference between ^{16}O and ^{18}O projectiles would be unlikely.

The calculated cross sections are too large for ^{10}Be (not shown), ^{14}C, ^{17}N and ^{17}O. For these isotopes, the separation energies used in the calculation of the Friedman probabilities P_f are particularly low and consequently the P_f values are high. In the calculation, 1.5 times as many events lead to the production of ^{14}C as of ^{14}N. The ratio of calculated cross sections, after renormalization by P_f, is 6.4 This increase is entirely due to the large P_f for ^{14}C(^{18}O $\rightarrow$ ^{14}C + ^{4}He). It seems as though the extreme alpha cluster structure implied by the Friedman model is somewhat less appropriate for ^{18}O than for ^{16}O or ^{20}Ne.

   e. The systems ^{12}C + ^{12}C, Ag, 85 MeV/A.

Figures 8 and 9 shows a comparison of calculated and experimental [36] cross sections for ^{12}C + ^{12}C and Ag at 85 MeV/A. In both cases, the calculated yields of ^{9}Be and ^{10}Be are too high. The same discrepancy appears in ^{16}O + ^{208}Pb at 2 GeV/A and ^{18}O + ^{48}Ti at 1.7 GeV/A. The neutron decay threshold of ^{9}Be is only 1.66 MeV, so a large fraction of the primary fragments may decay. There is no obvious reason for the ^{10}Be discrepancy, though.

f. N/Z ratios in the fragments.

As previously mentioned, at low beam energies heavy target nuclei produce larger yields of the neutron-excess PLF's than do light target nuclei which have a smaller neutron excess. The difference disappears at high energies. This observation has been explained by introducing pickup by the PLF's of some target neutrons [3]. This phenomenon certainly happens, for PLF's that contain more neutrons than the projectile are observed to be formed [2,37]. However, these extra yields of neutron-excess PLF's from ^{40}Ar + ^{197}Au compared with a target of ^{58}Ni are observed [30] at 44 MeV/A, somewhat beyond the Fermi energy, and the magnitude of the effect is as large as it is for 20 MeV/A ^{16}O, below the Fermi energy, on a target of ^{208}Pb [1]. In the system ^{20}Ne + ^{197}Au at 17 MeV/A, the more neutron-excess fragments of Li, Be and B are observed [22] to be slowed down, as they must be if they are at least in part formed from lighter isotopes by a neutron pickup process. This effect, though, is much weaker for heavier fragments.

Borrel et al. [37] observed fragments with one more neutron or proton than the projectle, but only in small yield. In the system ^{40}Ar + ^{27}Al at 44 MeV/A, the heavier fragments of a given Z are actually faster than the light fragments [38]. From a target of ^{197}Au, though, there is only a weak dependence of fragment velocity with mass at fixed Z [37]. These last two observations can be reproduced by the overlap model [39] without particle pickup.

The comparison of the calculated and experimental ratios of isotopic cross sections for ^{16}O + ^{208}Pb at 20 MeV/A and 2 GeV/A is shown in Table III. Using neutron/proton density ratios for ^{208}Pb that are everywhere equal to 126/82 (i.e. no neutron excess in the surface) gave the results shown in the second column of the Table. There is a small increase in the ratio for the neutron-excess isotopes, but it is much less than the experimental values shown in the last column. The middle column shows the effect of including a neutron-rich surface, using the Fermi density distribution parameters that are given in Table I. While the ratios never reach the large values observed experimentally, they are clearly in better agreement than those calculated without the neutron "skin".

While the comparison shows the importance of the use of a neutron-rich surface for the heavy target nuclei, there is still the possibility that some neutron pickup occurs at 20 MeV/A. It would be very interesting to make comparable comparisons for beam energies that are far enough above the Fermi energy that neutron pickup should be highly improbable, but at energies below about 150 MeV/A so that σ_{np} is still much larger than σ_{nn}. No experimental results are available to permit this comparison to be made. In the Monte Carlo model, the capture of scattered neutrons and protons by the PLF would probably increase the yield of neutron-rich PLF's from heavy targets, but this secondary process is not yet included in the calculations.

g. Spatial localization of the fragment production.

Figure 10 shows, for ^{16}O + ^{208}Pb at 20 MeV/A, a plot of the number of Monte Carlo events that produce a given PLF against the distance of closest

approach between the projectile and the target nuclei. It is clear that a given PLF is formed only in a narrow region of that distance. The calculation clearly reproduces the Friedman "spectroscopic factor". At a distance of closest approach where only one nucleon is scattered, there are only two possible PLF's − ^{15}N and ^{15}O. These therefore share the available cross section. For mass 8, though, there are many combinations of Z and N that add to 8, so that the number of events leading to any one of them − ^{8}Be for example − is correspondingly lower. The Friedman probability depending on separation energy is not included in the calculation of fig. 10.

The geometric overlap model [17] is very successful at predicting the elemental yields of PLF's at energies below 20 MeV/A. It assumes that PLF's of a given mass arise from a collision in which there is sufficient overlap between projectile and target to remove the appropriate amount of mass from the projectile. In addition, it assumes that the formation of PLF's occurs over a small region of impact parameters centered around that optimum value. The width of this region was treated as a parameter to be adjusted to obtain the best agreement with experiment. Figure 11 shows an overlap model calculation of the relative probability that a given ejectile will be formed at a given value of the distance of closest approach between ^{16}O and ^{208}Pb at 20 MeV/A. Again, the Friedman probability and "spectroscopic factor" are not included. The width of the distributions is the value that gave best agreement with experimental cross sections. A comparison of figs. 10 and 11 shows a remarkable similarity in the location in space of each PLF and also in the widths of the distributions. In both cases, the full width at half maximum is 1.6 fm. The arrows on fig. 10 mark the positions of the

maxima from fig. 11. Except for the formation of ^{1}H, the two results are barely distinguishable. The difference between the two calculations for the localization of ^{1}H comes from the use, in the Monte Carlo calculation, of small Pauli-blocked values for the nucleon-nucleon cross sections in the target interior. The overlap model is a "black nucleus" approximation which is equivalent to the use of large nucleon-nucleon cross sections at all target densities. The Monte Carlo calculations thus lend strong support to the assumptions that were made in the overlap model.

III. Summary of Conclusions.

A very simple microscopic calculation reproduces extremely well the energy dependence of reaction cross sections for nucleus-nucleus collisions in the energy range 10 MeV/A to 2 GeV/A. The values of the reaction cross section are sensitive only to the nucleon-nucleon scattering cross sections in the low density surface regions of the nuclei. Pauli blocking and Fermi motion are unimportant at low nuclear densities so that the free nucleon-nucleon cross sections can be used even at low projectile energies.

The cross sections for formation of particle-like fragments from ^{16}O + ^{208}Pb at 20 MeV/A and 2 Gev/A are in reasonably good agreement with experimental values, as are the fragment cross sections from ^{20}Ne + ^{197}Au at 20 MeV/A. Agreement for 1.7 GeV/A ^{18}O + ^{48}Ti and 85 MeV/A ^{12}C + ^{12}C, Ag is fairly good, but the calculation overestimates the yields of ^{9,10}Be.

The concentration of fragment yields towards the valley of stability, as observed experimentally, is assured by the use of the Friedman model of

fragment formation. It is not necessary to postulate large excitation energies in the primary fragments.

The enhanced yields of neutron-rich fragments that are observed experimentally from the collision of projectiles with heavy target nuclei at energies up to at least 44 MeV/A is due in part to the presence of a neutron-rich surface in the heavy nuclei. A part of the effect may be due to other mechanisms such as neutron pickup or recapture of scattered nucleons by the fragments.

The fragments of a given mass are formed from strongly localized regions of the distance of closest approach between the two colliding nuclei, the lighter fragments coming from the closer collisions.

IV. Acknowledgements.

TABLE CAPTIONS

Table I. Parameters used in the calculations. Part A shows the effective

nn(pp) and np cross sections used in the target center region and the free

values for the Coulomb-adjusted energy used in the surface. Part B shows the

neutron and proton density distributions in the Fermi distribution $\rho(R) =$

$\rho_0/[1 + \exp (R-c)/a]$. For ^{48}Ti – ^{208}Pb, the values of ρ_0, the

central density and a, the diffusivity, are from the Hartree-Fock-Strutinsky

calculations of Tondeur, Arcoragi and Pearson, ref. 19. The values of c were

calculated from ρ_0, a, and the neutron or proton number. For ^{12}C –

^{20}Ne, c was obtained from c $= 1.18A^{1/3}$ – 0.48 fm and a from electron

scattering rms radii. For ^{18}O, the ^{16}O proton and ^{20}Ne neutron

distributions were used.

Table II. Comparison of ejectile cross sections from ^{40}Ar + ^{12}C (213

MeV/A) and ^{40}Ar + ^{58}Ni (44 MeV/A). (refs 26 and 30 respectively). The

last columns show the abrasion model surface excitation energies for

fragments of mass 20, 25 and 30.

Table III. Comparison of ratios of ejectile cross sections for ^{16}O +

^{208}Pb at 20 MeV/A and 2 GeV/A. Columns labeled "No skin" and "Skin" are

Monte Carlo calculations without and with a neutron-rich surface for

^{208}Pb. The experimental results are from refs. 1 (20 MeV/A) and 31

(2GeV/A). Parameters of the calculations are given in Table I.

TABLE I.

PROJECTILE ENERGY (MeV/A,lab)	NUCLEON-NUCLEON CROSS SECTION (mb)			
	CENTER		FREE	
	σ_{nn}	σ_{np}	σ_{nn}	σ_{np}
10 } $^{12}C+^{12}C$	3	9	330	990
20 }	6.5	19.5	150	450
20 { $^{16}O+^{208}Pb$ $^{20}Ne+^{197}Au$	6.5	19.5	190	660
85	30	90	30	90
1700-2000	50	45	50	45

(A)

NUCLEUS	$\rho_O(p)$ (N/fm^3)	a(p) (fm)	c(p) (fm)	$\rho_O(n)$ (N/fm^3)	a(n) (fm)	c(n) (fm)
^{12}C	0.08468	0.521	2.222	0.08468	0.521	2.222
^{16}O	0.08468	0.521	2.511	0.08468	0.521	2.511
^{18}O	0.8468	0.521	2.511	0.08468	0.521	2.751
^{20}Ne	0.08468	0.521	2.751	0.08468	0.521	2.751
^{48}Ti	0.0800	0.506	3.826	0.0846	0.523	3.941
^{58}Ni	0.0792	0.500	4.199	0.0880	0.541	4.112
^{107}Ag	0.0724	0.494	5.222	0.090	0.569	5.223
^{197}Au	0.0638	0.459	6.557	0.0892	0.555	6.661
^{208}Pb	0.0632	0.457	6.557	0.0892	0.555	6.661

(B)

TABLE II.

EJECTILE	σ(mb) ^{12}C	^{58}Ni	ABRASION SURFACE ENERGY (MeV) ^{12}C	^{58}Ni
^{20}O	0.45	0.71		
^{20}F	16	19	150	34
^{20}Ne	23	30		
^{20}Na	0.3	–		
^{25}Ne	0.10	0.15		
^{25}Na	10	8.6	100	30
^{25}Mg	40	49		
^{25}Al	1.6	5.2		
^{30}Mg	0.12	0.38		
^{30}Al	4.3	2.2	58	23
^{30}Si	50	55		
^{30}P	9	12		

TABLE III.

EJECTILE	$\dfrac{\sigma(20\ \text{MeV/A})}{\sigma(2\ \text{GeV/A})}$		
	NO SKIN	SKIN	EXPT.
^6Li	0.93	0.91	$1.0^{+.4}_{-.3}$
^7Li	1.2	0.98	$2.4^{+.9}_{-.6}$
^8Li	1.4	3.0	-
^7Be	0.61	0.51	$0.35^{+.25}_{-.1}$
^9Be	1.1	1.4	$3.5^{+1.8}_{-.7}$
^{10}Be	1.2	1.8	6.0^{+3}_{-2}
^{11}Be	1.5	2.6	-
^{10}B	1.1	0.89	$1.6\pm.8$
^{11}B	0.96	1.1	$2.2^{+.8}_{-.4}$
^{12}B	1.2	1.9	$6.0^{+2.4}_{-3.3}$
^{13}B	0.91	2.2	-
^{11}C	0.76	0.67	$0.75^{+.2}_{-.4}$
^{12}C	0.85	0.88	1.6 ± 4
^{13}C	1.0	1.2	$2.8^{+.7}_{-.9}$
^{14}C	1.1	1.5	$3.5^{+.8}_{-2}$
^{13}N	0.75	0.55	$1.7^{+.5}_{-.9}$
^{14}N	0.79	0.76	$2.0\pm.8$

REFERENCES

1. G. K. Gelbke et al., Physics Reports $\underline{42}$ No 5 (1978) 312.

   M. Buenerd et al., Phys. Rev. Lett. $\underline{37}$ (1976) 1191.

2. Ch. Egelhaaf et al., Nucl. Phys. $\underline{A405}$ (1983) 397.

3. H. Homeyer, Nuclear Science Research Conference Series, Vol. 6 p. 95, "Nuclear Physics with Heavy Ions", Harwood Academic Publishers, 1984.

4. R. M. DeVries and J. C. Peng, Phys. Rev. Lett. $\underline{43}$ (1979) 1373.

5. N. J. DiGiacomo, R. M. DeVries and J. C. Peng, Phys. Rev. Lett. $\underline{45}$ (1980) 527.

6. R. M. DeVries and J. C. Peng, Phys. Rev. $\underline{C22}$ (1980) 1055.

7. N. J. DiGiacomo, J. C. Peng and R. M. DeVries, Phys. Lett. $\underline{101B}$ (1981) 383.

8. J. C. Peng, R. M. DeVries and N. J. DiGiacomo, Phys. Lett. $\underline{98B}$ (1982) 244.

9. H. Bertini, Phys. Rev. $\underline{C5}$ (1973) 2118.

10. A. J. Cole, Report ISN 84.35, Grenoble, Aug. 1984.

11. P. J. Karol, Phys. Rev. $\underline{C11}$ (1975) 1203.

12. J. P. Jeukenne, A. Lejeune and C. Mahaux, Phys. Rev. $\underline{C16}$ (1977) 80.

13. J. W. Tanahata et al, Phys. Lett. $\underline{100B}$ (1981) 121.

14. J. W. Negele and D. Vautherin, Phys. Rev. $\underline{C5}$ (1972) 1472.

15. B. Sinha, Phys. Rev. Lett. $\underline{50}$ (1983) 91.

16. W. A. Friedman, Phys. Rev. $\underline{C27}$ (1983) 569.

17. B. G. Harvey and H. Homeyer, LBL Report 16882, submitted to Phys. Lett.

18. C. Perrin et al., Phys. Rev. Lett. $\underline{49}$ (1982) 1905 and references therein.

19. F. Tondeur, J. P. Arcoragi and J. M. Pearson, Contribution to the International Workshop on Semiclassical Methods in Nuclear Physics, Institut Laue-Langevin, Grenoble, 1984.

20. S. Kox et al., Nucl. Phys. A420 (1984) 162.

21. V. Borrel, Thesis, Université Paris-Sud (Orsay), March 1984.

22. R. G. Stokstad et al., LBL Report 18240, presented at International Conference on Heavy Ion Physics, Mt Fuji, Japan, Aug. 1984.

23. M. J. Murphy et al., Phys. Lett. 120B (1983) 319.

24. W. D. M. Rae et al., Phys. Rev. C30 (1984) 158.

25. D. J. Morrissey et al., Phys. Rev. C18 (1978) 1267.

26. Y. P. Viyogi et al., Phys. Rev. Lett. 42 (1979) 33.

27. W. D. Myers et al., Phys. Rev. C15 (1977) 2032.

28. L. F. Oliviera, et al., Phys. Rev. C19 (1979) 826.

29. J. Hüfner, K. Schäfer and B. Schürmann, Phys. Rev. C12 (1975) 1888.

30. D. Guerreau et al., Phys. Lett. 131B (1983) 293, and M. Lefort (private communication).

31. D. L. Olson et al., Phys. Rev. C28 (1983) 1602.

32. H. Fuchs et al., HMI Berlin Report 308 84, submitted to Phys. Rev. C.

33. H. Homeyer et al., Z. Phys. A319 (1984) 143.

34. H. Homeyer et al., Phys. Rev. C26 (1982) 1335.

35. D. L. Olson et al., Phys. Rev. C24 (1981) 1529.

36. H. Ryde, Physica Scripta, T5 (1983) 114.

37. V. Borrel et al., Z. Phys. A 314 191 (1983).

38. J. Barrette et al., Saclay Report No. 2135, March 1984.

39. B. G. Harvey and M. J. Murphy, Phys. Lett. 130B (1983) 373.

FIGURE CAPTIONS

Fig. 1. The nucleon-nucleon total cross sections.

Fig. 2. The collision geometry used in the Monte Carlo calculations.

Fig. 3. Comparison of Monte Carlo calculations (●) with experimental measurements (o) of the reaction cross section σ_r for ^{12}C ^{12}C. The dashed line is the calculation of ref. 8.

Fig. 4. Abrasion model surface energy for ^{40}Ar + ^{12}C and ^{58}Ni. According to the model, the lightest primary ejectile from ^{40}Ar + ^{12}C has mass number 16.

Fig. 5. Comparison of calculated primary fragment cross sections (dashed lines) with inclusive experimental cross sections for ^{16}O + ^{208}Pb at 20 MeV/A (ref. 1), Part A, and 2 GeV/A (ref. 31), Part B. The parameters used in the calculation are given in Table I. Symbols: ▦ He, ● Li, ▲ Be, ☐ B, o C, ▽ N, ◇ O.

Fig. 6. Comparision of calculated primary fragment cross sections (dashed lines) with inclusive experimental cross sections (ref. 2) for ^{20}Ne + ^{197}Au at 20 MeV/A. The parameters used in the calculation are given in Table I. Symbols as in fig. 5.

Fig. 7. Comparison of calculated primary fragment cross sections (dashed lines) with inclusive experimental cross sections (ref. 35) for ^{18}O + ^{48}Ti at 1.7 GeV/A. The parameters used in the calculation are given in Table I. Symbols as in fig. 5.

Fig. 8. Comparison of calculated primary fragment cross sections (dashed lines) with inclusive experimental cross sections (ref. 36) for ^{12}C + ^{12}C at 85 MeV/A. The parameters used in the calculation are given in Table I. Symbols as in fig. 5.

Fig. 9. Comparison of calculated primary fragment cross sections (dashed
 lines) with inclusive experimental cross sections (ref. 36) for
 ^{12}C + Ag at 85 MeV/A. The parameters used in the calculation are
 given in Table I. Symbols as in fig. 5.

Fig. 10. Spatial localization of fragment sources for ^{16}O + ^{208}Pb at 20
 MeV/A – Monte Carlo calculation.

Fig. 11. Spatial localization of fragment sources for ^{16}O + ^{208}Pb at 20
 MeV/A – overlap model of ref. 17.
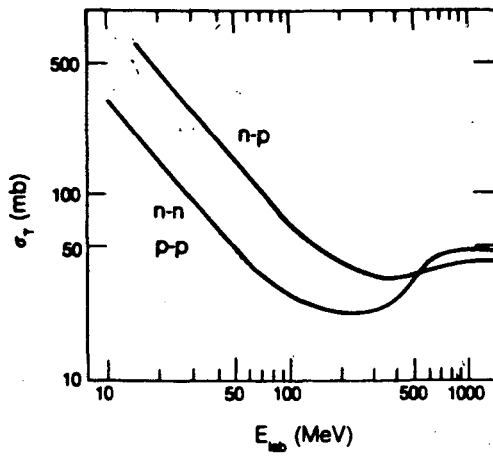
Fig. 1

XBL 844-9327
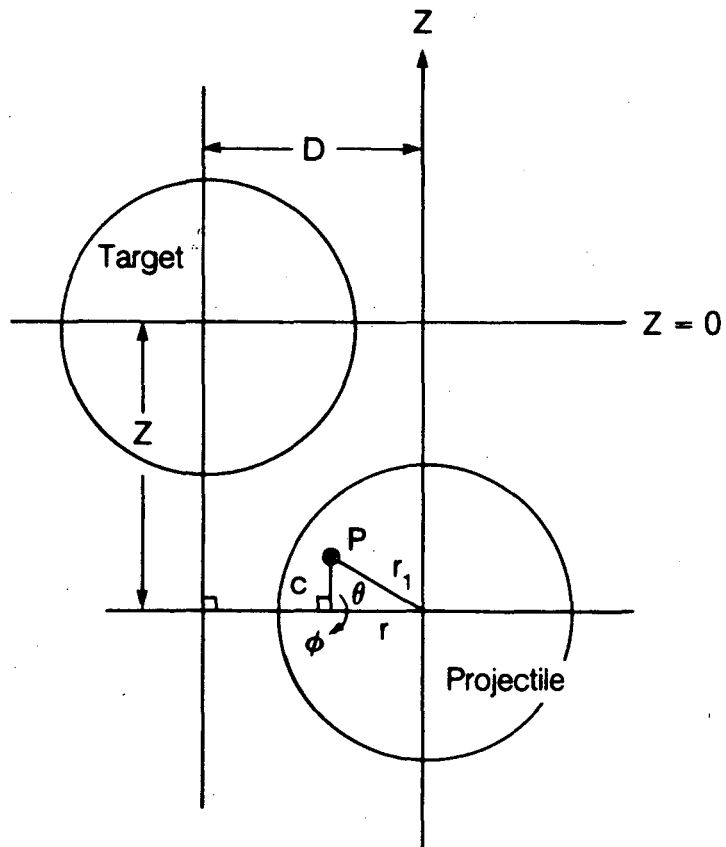
Fig. 2

XBL 844-9324
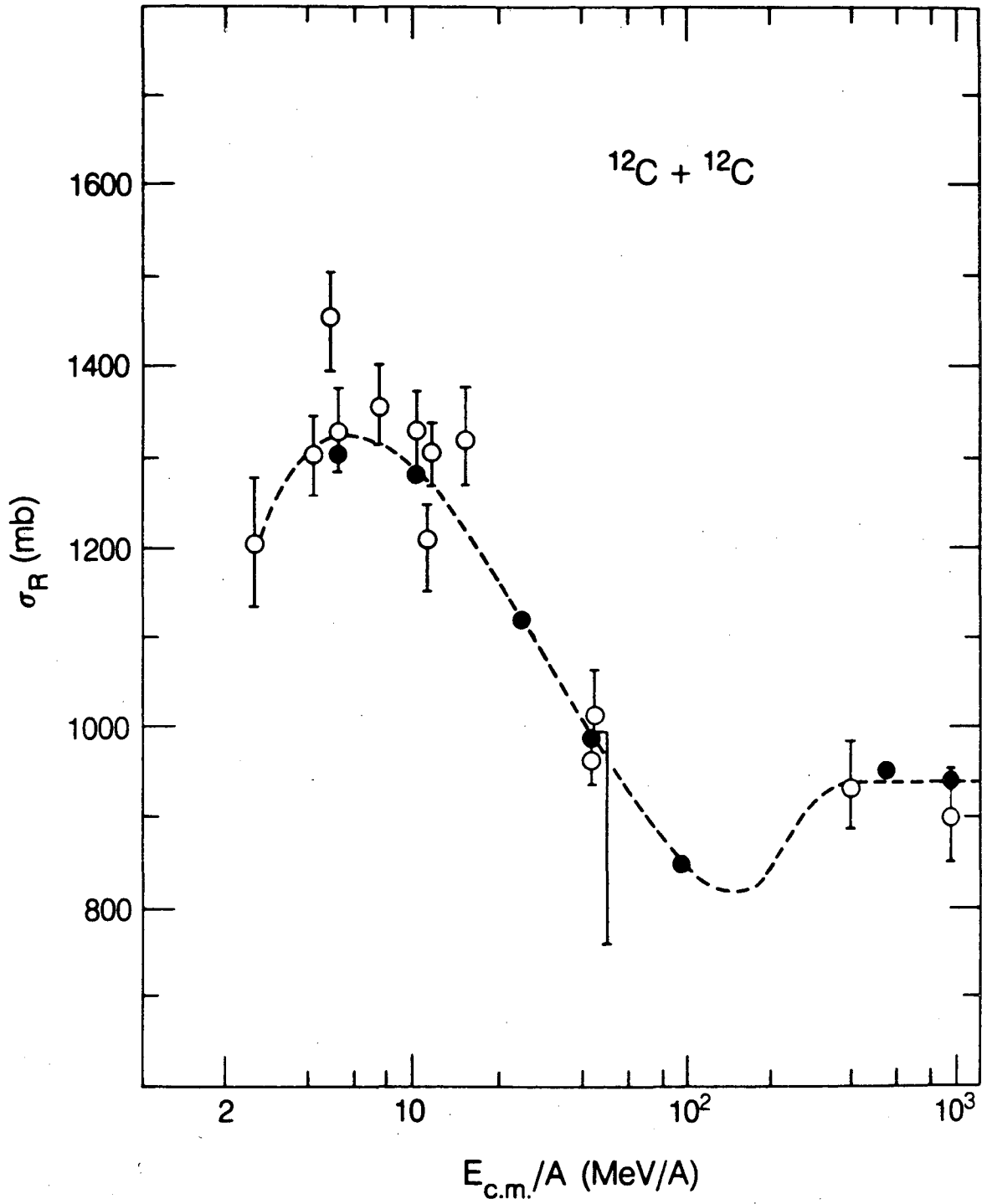
Fig. 3

XBL 844-9325
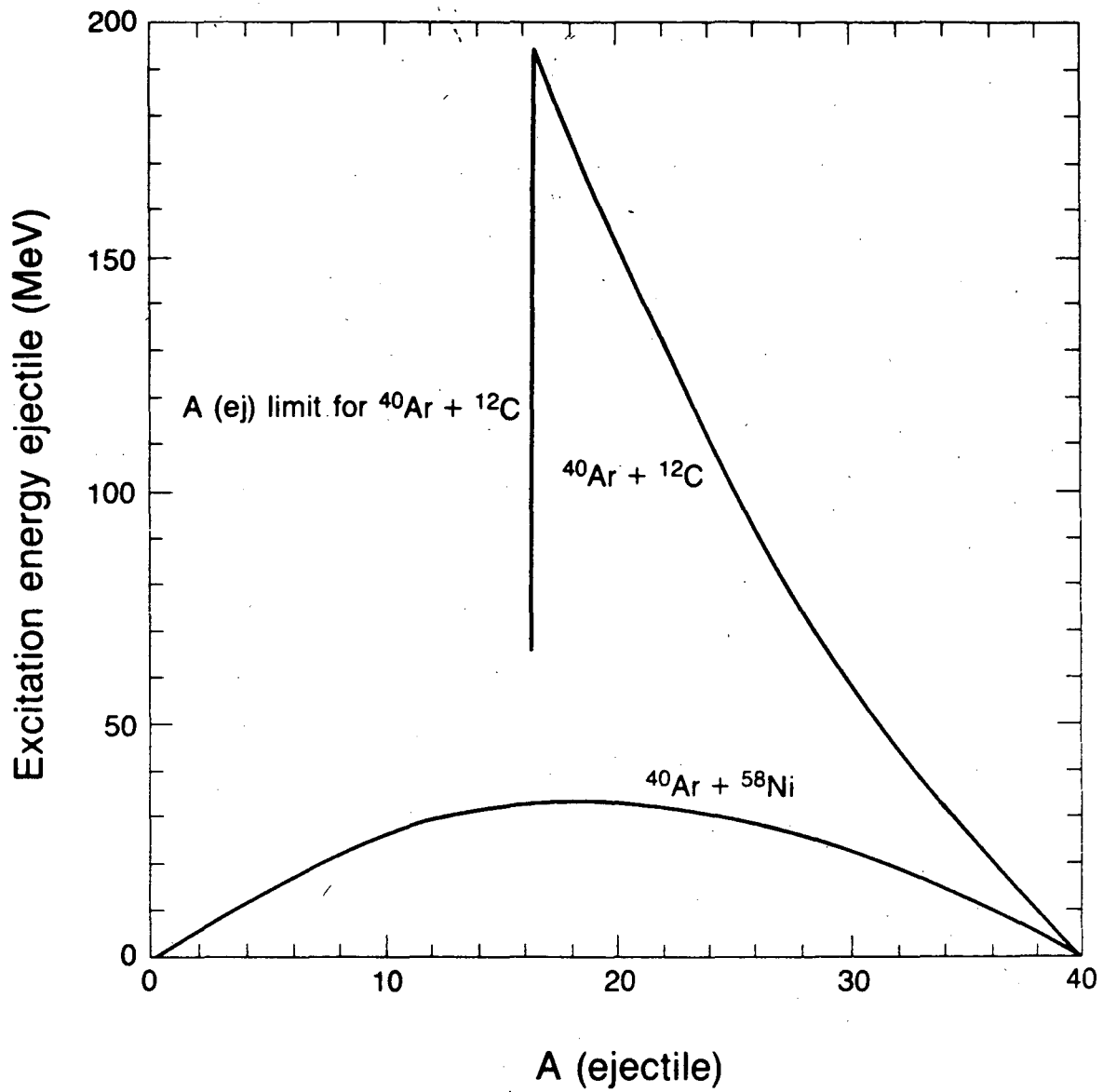
Fig. 4
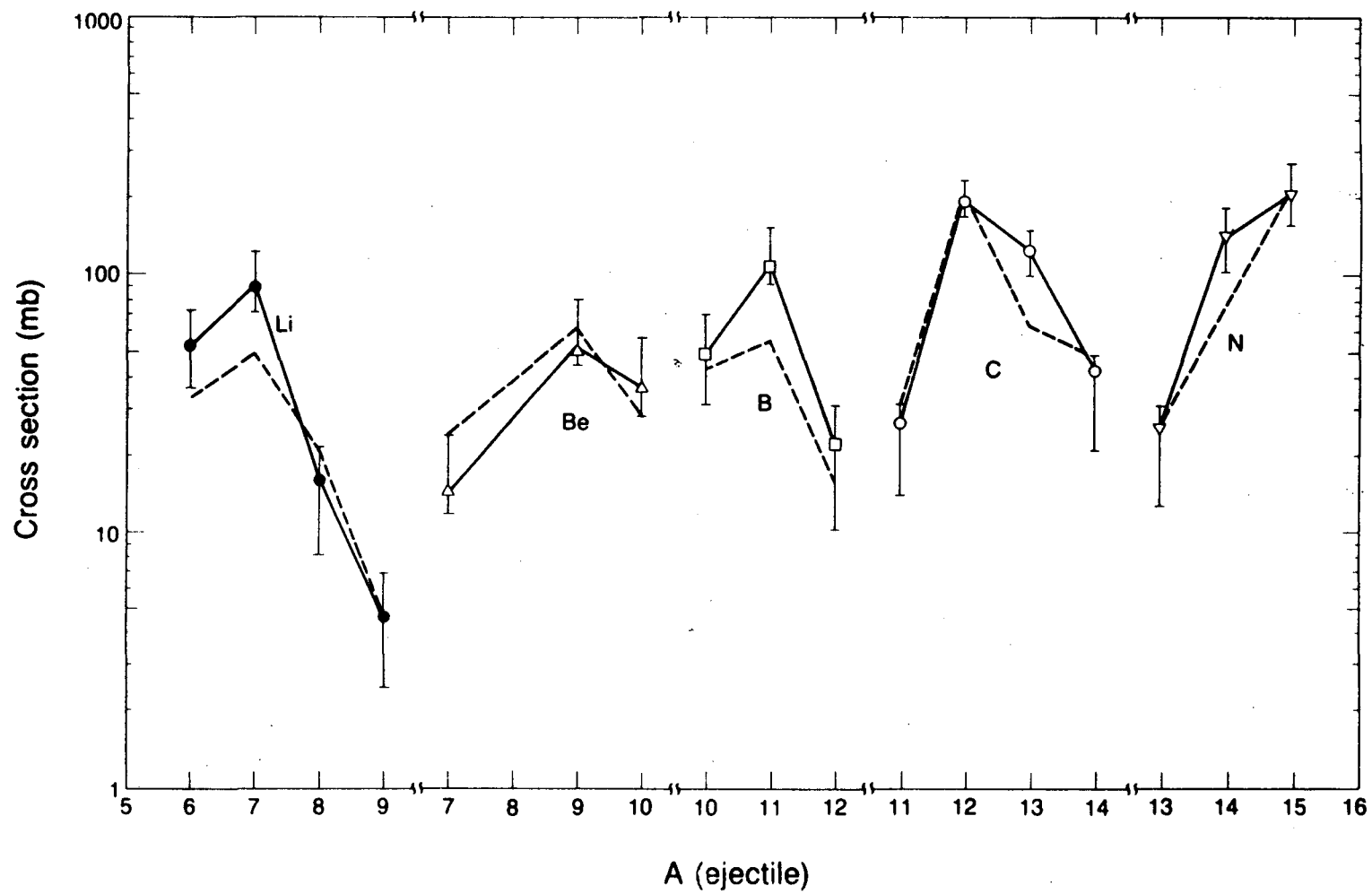
XBL 852-6989

Fig. 5A

XBL 862-8990

Fig. 5B

XBL 852-7007

-36-
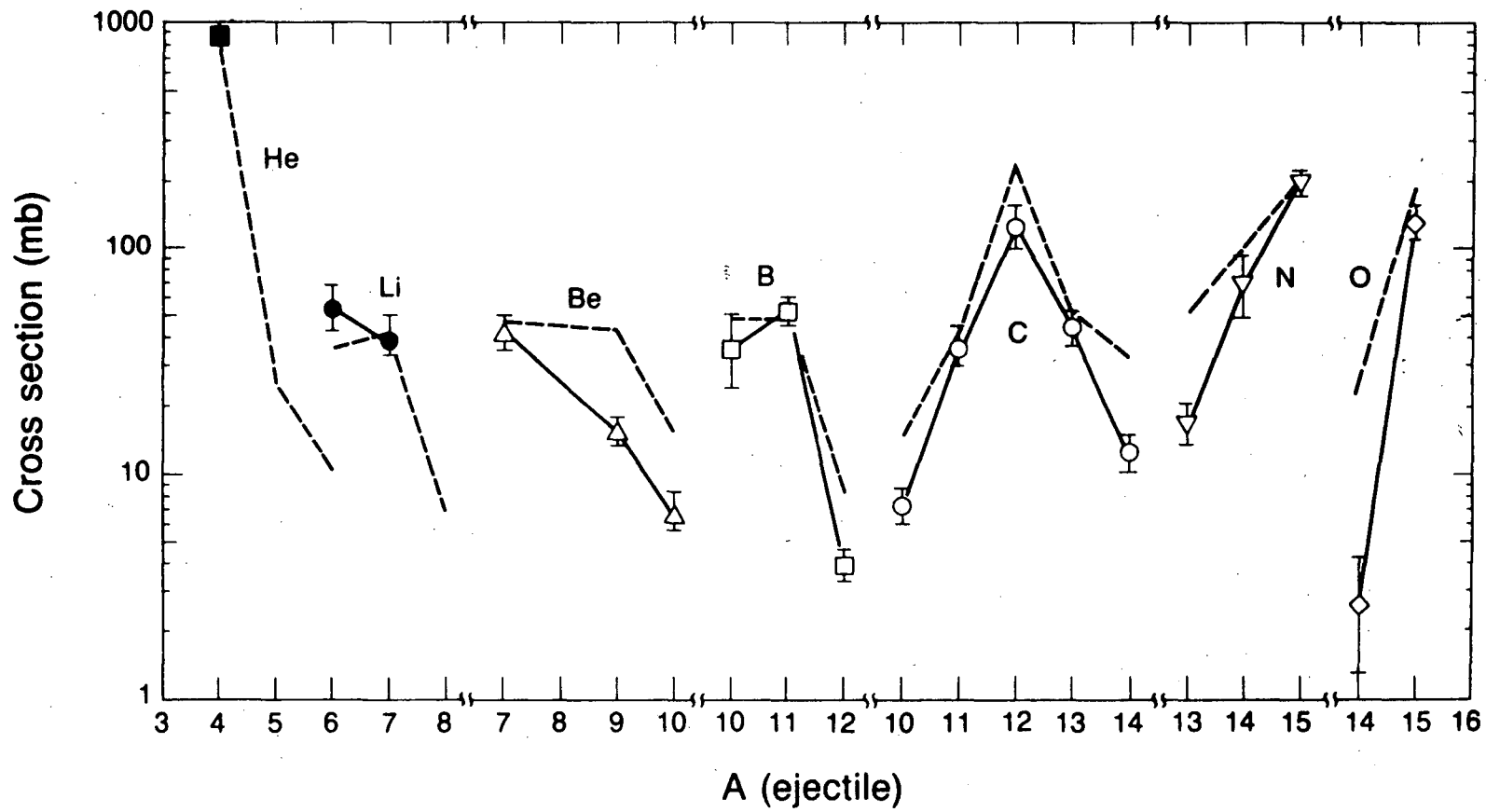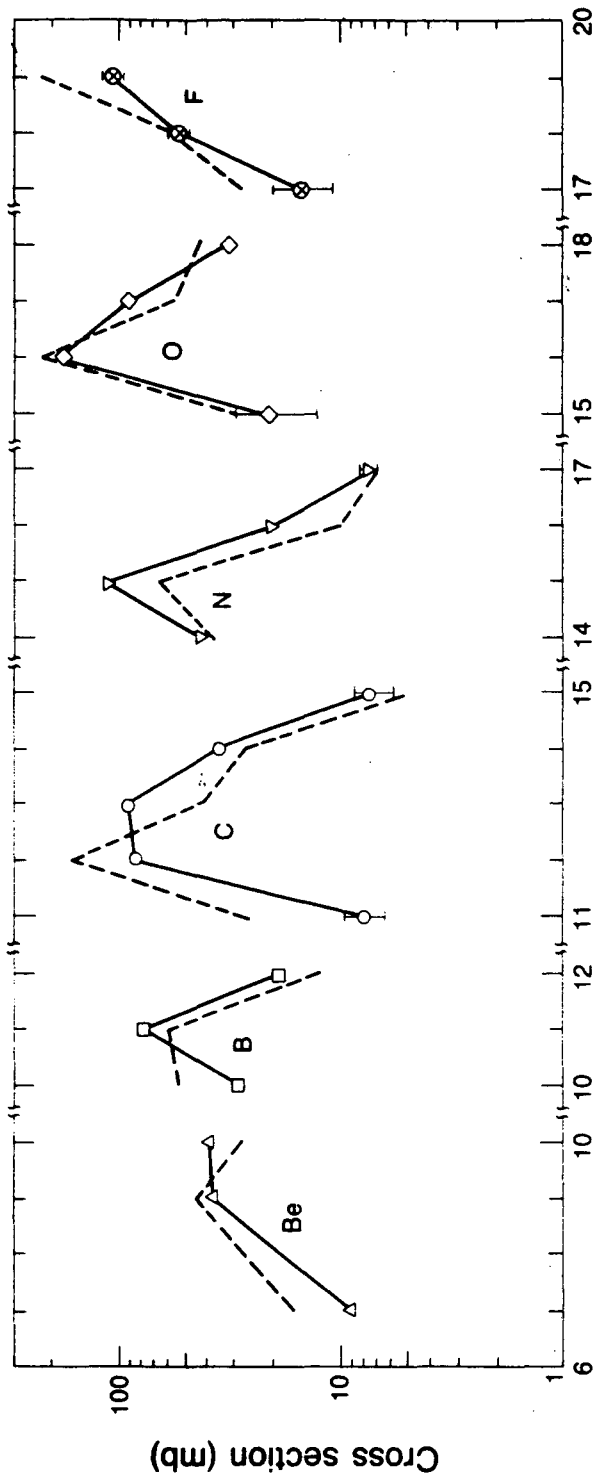
Fig. 6
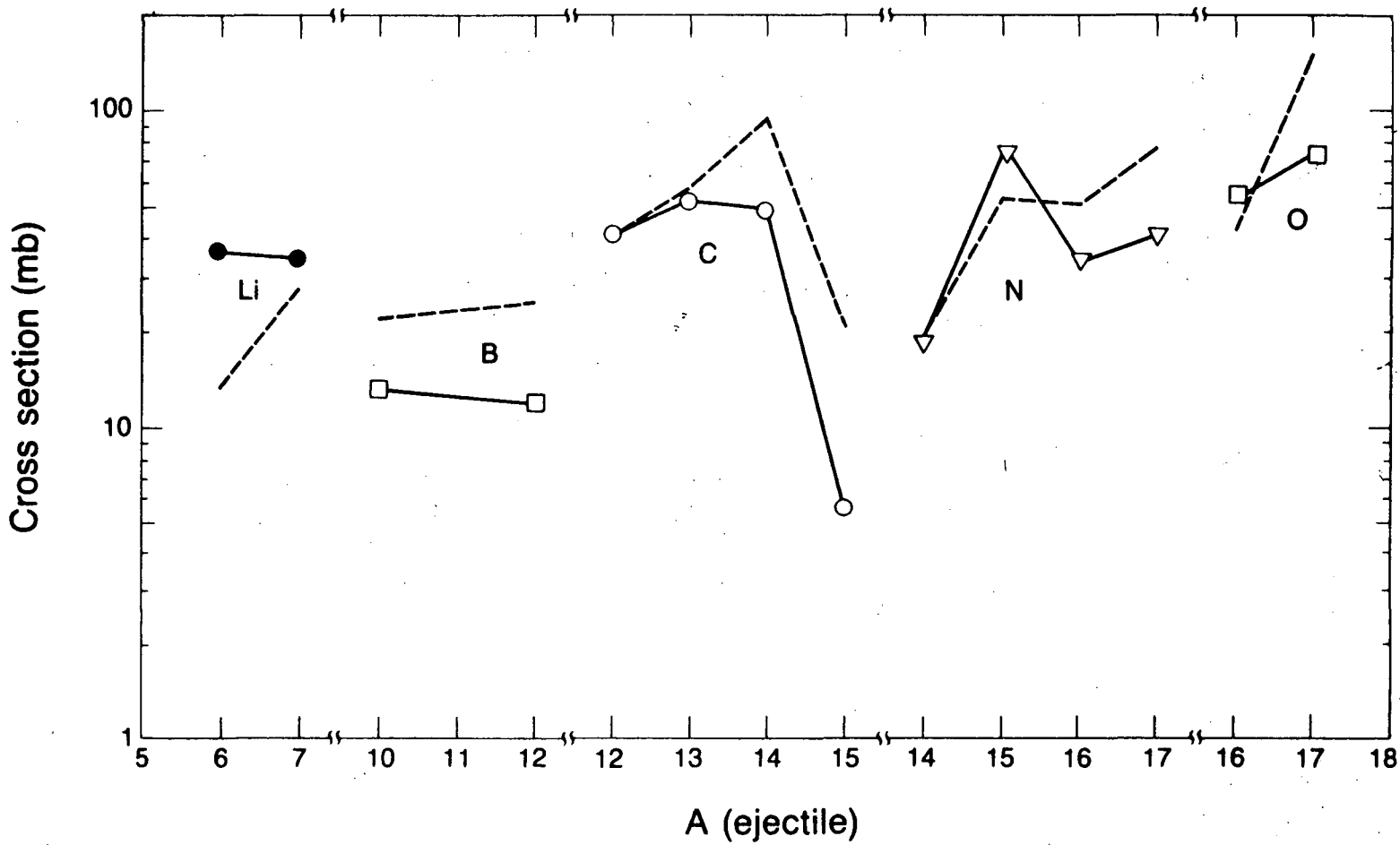
XBL 852-6991

Fig. 7

XBL 852-7008

Fig. 8

XBL 852-6986
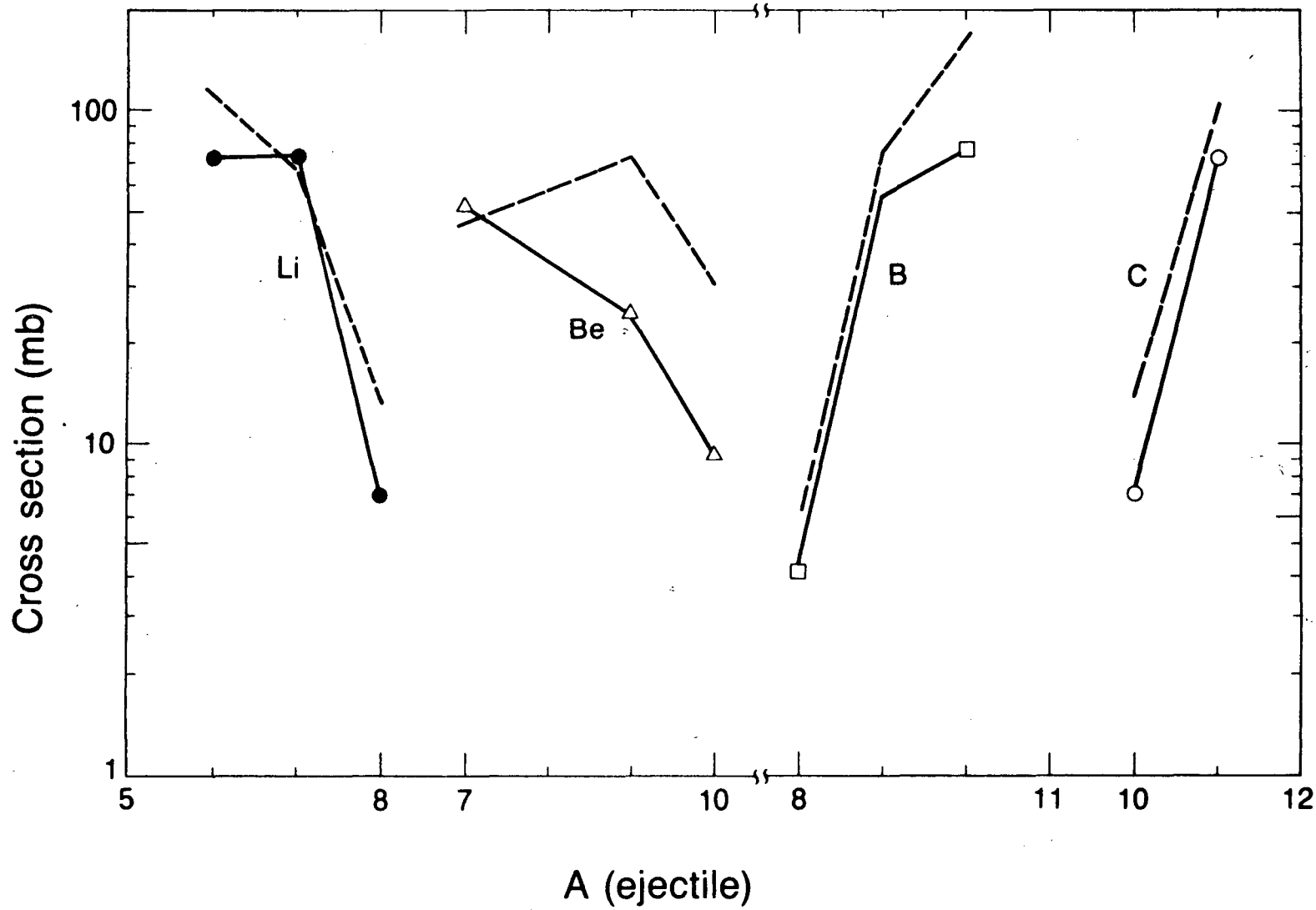
Fig. 9
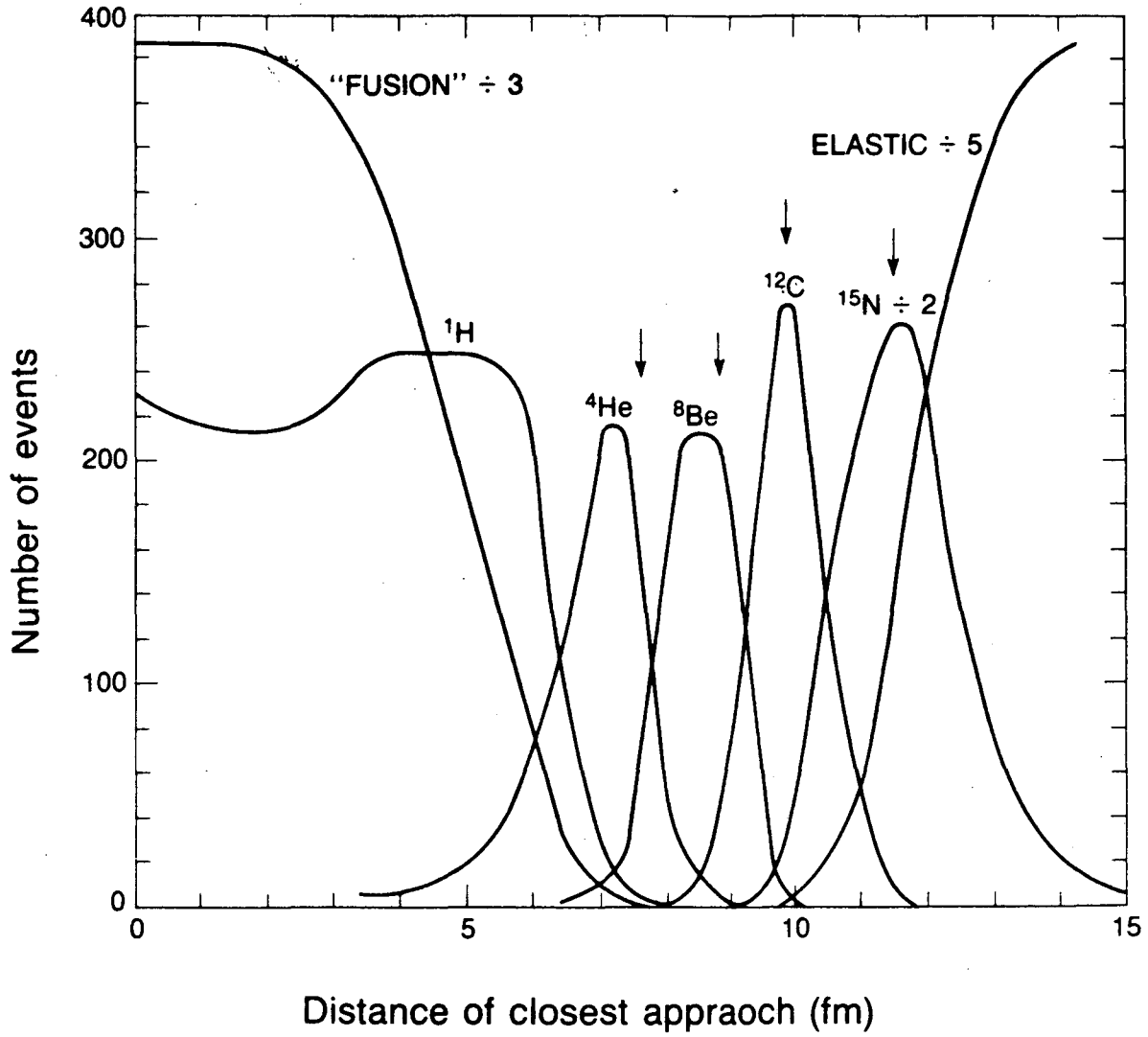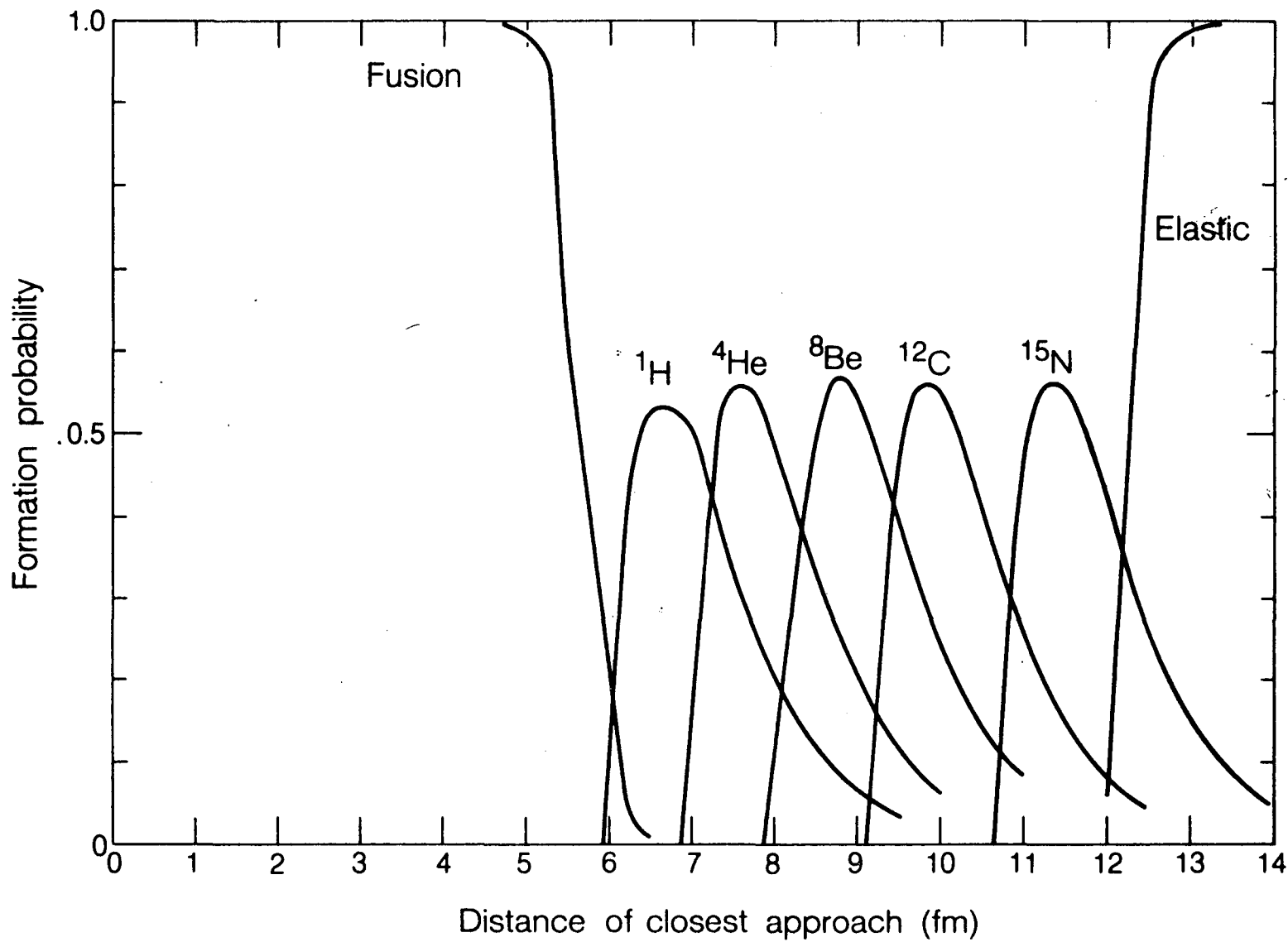
-40-

Fig. 10

XBL 852-6988

Fig. 11

XBL 844-9328

TECHNICAL INFORMATION DEPARTMENT
LAWRENCE BERKELEY LABORATORY
UNIVERSITY OF CALIFORNIA
BERKELEY, CALIFORNIA 94720